Mechatronics 47 (2017) 97–104

Contents lists available at ScienceDirect

Mechatronics

journal homepage: www.elsevier.com/locate/mechatronics

Technical note

Positive acceleration, velocity and position feedback based damping control approach for piezo-actuated nanopositioning stages☆

Linlin Li, Chun-Xia Li, Guoying Gu*, Li-Min Zhu

State Key Laboratory of Mechanical System and Vibration, School of Mechanical Engineering, Shanghai Jiao Tong University, Shanghai, 200240, China

ARTICLE INFO

Article history:
Received 18 October 2016
Revised 10 July 2017
Accepted 6 September 2017

Keywords:
Nanopositioning stages
Piezoelectric actuators
Hysteresis compensation
Damping control
Positive acceleration velocity and position feedback

ABSTRACT

This paper proposes a new damping control approach with positive acceleration, velocity and position feedback (PAVPF) scheme for piezo-actuated nanopositioning stages to implement high-bandwidth operation. To achieve this objective, the intrinsic hysteresis nonlinearity of the piezoelectric actuator is firstly handled by a feedforward compensator with a modified Prandtl–Ishlinskii model. Afterwards, the PAVPF controller with the pole-placement method is implemented to suppress the lightly damped resonant mode of the hysteresis compensated system. With the PAVPF controller, the poles of the damped system in a third-model can be placed to arbitrary positions with an analytical method. Finally, for accurately tracking a predefined trajectory, a high-gain proportional-integral (PI) controller is designed, which could deal with the disturbance and the unmodeled dynamics. For verifying the proposed PAVPF-based control approach, comparative experiments with positive velocity and position feedback controller and with PI controller are conducted on a piezo-actuated nanopositioning stage. Experimental results demonstrate that the developed control approach with PAVPF controller is effective on damping control and improves the control bandwidth of the conventional PI controller from 111 Hz to 766 Hz, which leads to the significant increase of the tracking speed.

1. Introduction

Nowadays, piezo-actuated nanopositioning stages are intensively required in industrial devices including the scanning probe microscopes [1–3], and micromanipulators [4,5]. The key components of these nanopositioning stages are the piezoelectric actuators (PEAs) and flexure hinge based mechanisms. However, there are two main challenges that limit the improvement of the tracking accuracy and speed of such stages [6–8]. One is the inherent hysteresis nonlinearity of the PEAs, which causes the conventional control approaches for linear dynamic systems inapplicable [9]. The other one is the lightly damped resonant behavior of the mechanisms, which generally restricts the maximum operation frequency less than the 1%–10% of its resonance frequency of the stage [10,11].

For the decades past, many efforts have been made to eliminate the inherent hysteresis behavior of the PEAs. Charge actuation [12] is a feasible method in mitigating hysteresis. However, the additional cost and the greater circuit complexity hinder it from being widely used until now. Among the methods in voltage-actuation case, the feedforward control with a hysteresis compensator [13] has been demonstrated to be effective to cancel the hysteresis, which has been extensively employed in the literature [14–17].

To address the lightly damped resonant behavior, several damping control techniques have been reported [7,18–29]. With the capacity to manage modeling uncertainties and the robustness to parameter variations, the feedback damping control has become promising, such as the integral resonant control [24,25], the force feedback control [23], and the positive position feedback (PPF) control [18]. Due to the lack of the force sensor in many apparatuses, the force feedback control has not been used intensively. With the simple structure and the ability to place the poles of the damped system to more benefitting locations [18], the PPF controller is widely used to suppress the vibrations of piezo-actuated systems [28,29]. Moreover, based on the PPF technique, several works have been extended for vibration suppression in multimode condition and/or disturbance decay, such as the hybrid positive feedback control [20], and the modified positive position feedback control [22]. It should be noted that the poles of the damped system with a PPF controller or the extended controllers could not be placed arbitrarily [21,28]. Hence, the positive velocity and position feedback (PVPF) control [21] is designed to suppress the undesired vibra-

☆ This paper was recommended for publication by Associate Editor Dr Garrett Clayton.

* Corresponding author.
E-mail addresses: guguoying@sjtu.edu.cn, guguoying@gmail.com (G. Gu).

https://doi.org/10.1016/j.mechatronics.2017.09.003
0957-4158/

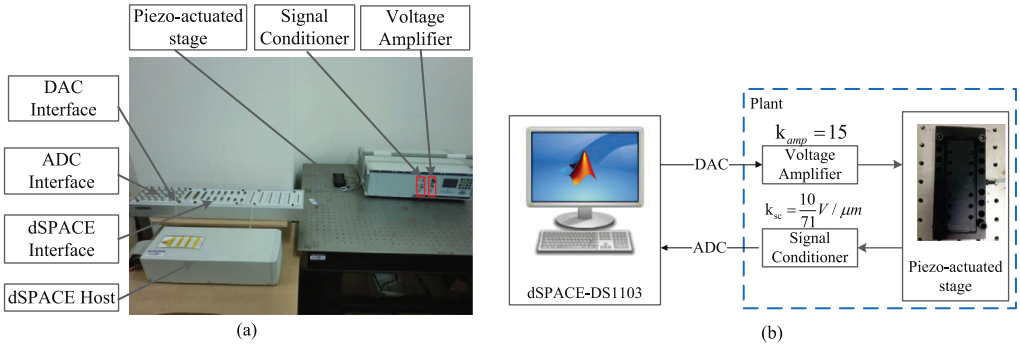

Fig. 1. The experimental platform: (a) the experimental setup; (b) the block diagram.

tion of a second-order system, which makes it possible to assign the poles of the damped system to arbitrary locations. The PVPF [21] controller is an effective method for damping control and has been extensively employed to nanopositioners, such as [21,26]. It is worthy of mentioning that these damping control techniques are generally effective for the system with a typical second-order model to implement arbitrary poles placement. However, in general, the dynamic model of the piezo-actuated nanopositioning stages is third-order [11], which has also been confirmed by various experiments [11,27,30]. In this sense, the analytical method for designing PVPF controller is not applicable for such third-order system. Of course, the numerical method may be employed to find the optimum control parameters for designing PVPF controller. Therefore, inspired by the reported PVPF controllers, the objective of this work is to develop a damping controller for the third-order dynamic model such that the poles of the damped system can be assigned arbitrarily.

In this paper, a positive acceleration, velocity and position feedback (PAVPF) control approach is proposed to damp the undesired resonant mode of a piezo-actuated nanopositioning stage with a third-order model. The developed control approach can be implemented with three steps. Firstly, due to hysteresis nonlinearity of the PEA, a direct inverse feedforward compensator is utilized, which leads to an approximately linear system. Secondly, the PAVPF control approach is presented to suppress the vibration of the compensated system with an analytical method. The pole-placement method is used to design the PAVPF controller. Thirdly, a feedback tracking controller is designed to cope with the disturbance and the unmodeled dynamics. As we mentioned above, the PVPF controller may not be used to arbitrarily set the poles with an analytical method for the third-order system. In order to make a comparative test between the PVPF controller and PAVPF controller, a numerical algorithm is applied in this work. On the other hand, with the PAVPF controller, the poles of the damped system are able to be placed arbitrarily, depending on the designers. In the end, comparative experiments with PVPF controller and with conventional PI controller are performed to validate the proposed control approach.

The remainder of this paper is arranged as follows. Section 2 describes the experimental platform. In Section 3, the proposed PAVPF-based control approach is designed and comparative experiments with PVPF controller are conducted. In Section 4, real-time experimental results are presented and the conclusion is drawn in the last section.

2. System description

The experimental platform used in this work is shown in Fig. 1(a). As an example, a piezo-actuated nanopositioning stage (produced by Harbin Core Tomorrow Science and Technology Co., Ltd) is utilized. The one dimensional flexure-guided piezo-actuated nanopositioning stage is composed of three parts: an integrated high-resolution strain gauge sensor, a flexure hinge guiding mechanism with the travel range of 71.55 μm , and a PEA to drive the mechanism. The PEA in this device is made of piezoceramic. The external size of the stage is $132 \times 50 \times 25$ mm. A voltage amplifier with the constant amplification factor of 15 is provided to drive the PEA. The signal conditioner is used to capture the position signal from the sensor of the stage for parameter identification and closed-loop control. The dSPACE system, with 16-bit ADCs and 16-bit DACs interface in the board, is used to carry out the control approach in the environment of Simulink/Matlab by the software of ControlDesk. The ADC interface is used to capture the actual position signal from the signal conditioner and convert it to digital voltage signal. The DAC interface is employed to convert the digital signal generated by the computer to analogue excitation voltage signal and transfer it to the amplifier. In this work, the output voltage of the dSPACE is set to range from 0 to 10 V, and the sampling rate of the control system is chosen as 20 kHz. Fig. 1(b) shows the experimental platform schematically.

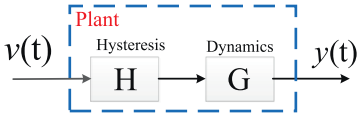

Fig. 2. The block diagram of the Hammerstein-like model.

3. Controller design

Before the design of the PAVPF-based controller, the dynamics of the nanopositioning stage is studied. In general, a Hammerstein-like model can describe the dynamic behavior of the stage, which cascades the rate-independent hysteresis nonlinearity with the linear dynamics of the system [11,31,32]. Fig. 2 schematically shows the Hammerstein-like model, where H represents the rate-independent hysteresis nonlinearity, and G contributes the plant linear dynamic model.

Taking into account that the proposed PAVPF-based controller is tailored for a linear system, the hysteresis nonlinearity H hampers its design and application. To address this issue, a feedforward compensator will be designed firstly to handle the hysteresis behavior of PEAs.

3.1. Hysteresis compensator

To cancel the hysteresis behavior, the feedforward compensator is widely used in the voltage actuation case. With the model simplicity and exclusion of the inversion-model calculation, a direct inverse hysteresis compensation method is applied in this work,

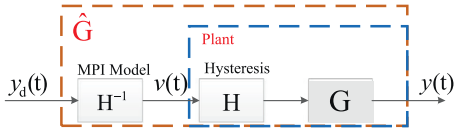

Fig. 3. The block diagram of the system with the feedforward compensator.

Table 1
The obtained parameters of the feedforward compensator.

Number	r_i	c_i	p_i
1	0	−0.60888	0.12836
2	0.1	−0.39862	1.91854
3	0.2	−0.00259	
4	0.3	−0.04132	
5	0.4	−0.01665	
6	0.5	−0.00100	
7	0.6	−0.05216	
8	0.7	−0.02983	
9	0.8	−0.00791	
10	0.9	−0.64570	

based on a modified Prandtl–Ishlinskii (MPI) model [33]. The block diagram of the system with the hysteresis compensator H^{-1} is shown in Fig. 3, where $y_d(t)$ represents the desired trajectory, $v(t)$ denotes the control signal of the feedforward compensator, and $y(t)$ represents the real displacement signal of the stage.

Based on the MPI model [33], the output of the feedforward compensator can be expressed as

$$v(t) = p_1 y_d^3(t) + p_2 y_d(t) + \sum_{i=1}^{N} c(r_i) F_{r_i}[y_d](t) \tag{1}$$

where p_1 and p_2 are the constant coefficients of the input polynomial, $c(r_i)$ is the weight of each play operator $F_{r_i}[y_d](t)$, N is the number of the used play operators. $F_{r_i}[y_d](t)$ is a one-side play operator

$$\begin{aligned} F_{r_i}[y_d](0) &= \max(y_d(0) - r_i, 0) \\ F_{r_i}[y_d](t) &= \max(y_d(t) - r_i, \min(y_d(t), F_{r_i}[y_d](t - T_s))) \end{aligned} \tag{2}$$

where T_s is the sampling period, and r_i is the threshold value. In this work, the fixed threshold value r_i is chosen as:

$$r_i = \frac{i}{N} ||y_d(t)||_\infty, \quad i = 0, 1 \ldots N-1 \tag{3}$$

N is selected as 10 in this work. To identify the parameters, a multi-value triangular signal in a relatively low frequency is used to stimulate the system, without triggering the dynamics of the system. With the corresponding input and output of the system captured, the parameters of the feedforward compensator in (1) can be optimized with a modified particle swarm optimization method [34]. All the obtained parameters are shown in Table 1. The readers may refer to [33,34] for the detailed algorithms of parameters optimization. Fig. 4(a) displays the hysteresis compensation results of the piezo-actuated stage with the feedforward compensator, where an approximately linear relationship is observed. Moreover, Fig. 4(b) provides the response of the stage without the feedforward compensator, where obvious hysteresis occurs. It is demonstrated that the inherent asymmetric hysteresis nonlinearity has been significantly reduced with the feedforward hysteresis compensator. Therefore, the compensated system $\hat{G}$ can be approximately considered to be linear.

3.2. PAVPF damping controller

Here, the design of the PAVPF controller is presented. Firstly, the dynamic model $\hat{G}$ needs to be identified. To this end, a band-limited white noise signal is utilized to stimulate the compensated system. The System Identification Toolbox of Matlab is used for determining the transfer function of the compensated system, based on the corresponding system output position signal and the input noise signals. The identified model $\hat{G}$ has the transfer function of

$$\hat{G}(s) = \frac{a_3 s^3 + a_2 s^2 + a_1 s + a_0}{s^3 + b_2 s^2 + b_1 s + b_0} \tag{4}$$

where $a_3 = 0$, $a_2 = 815.3$, $a_1 = -1.783e7$, $a_0 = 2.974e11$, $b_2 = 4948$, $b_1 = 1.032e8$, $b_0 = 2.723e11$. With the identified model in Eq. (4), it is convenient to obtain the original poles of $\hat{G}$, which are

$$p_{1,2} = -1054 \pm 9806i \tag{5}$$

$$p_3 = -2840 \tag{6}$$

It can be obtained that the damping ratio of the system is 0.107, which is a definitely lightly damped resonant mode. To illustrate the preciseness of the identified dynamic model, Fig. 5 compares the frequency responses of the experimental results and the simulation results. It is observed that the identified model accurately describes the dynamic behavior of the system. In addition, there is a lightly damped undesired resonant mode of the compensated system, which restricts the improvement of the tracking speed of the stage.

Remark: we should mention that, in general, the numerator of G(s) is third order when developing the PAVPF controller. However, in this work, the numerator of G(s) in the identified model is second-order, which is just a special case. Therefore, we adopt $a_3 = 0$ in Eq. (4) for verification. Without losing generality, the design method is still available when $a_3 \neq 0$.

To damp the resonant mode of the compensated system, the PAVPF controller will be designed. The block diagram of the proposed PAVPF controller is shown in Fig. 6. The output of the PAVPF controller $u_p(t)$ is the synthesis of acceleration, velocity and position signals based on the system output, and $u_p(t)$ is positively feedback to the compensated system $\hat{G}$. The transfer function of the PAVPF controller can be written as

$$C_{damp}(s) = \frac{\Gamma_2 s^2 + \Gamma_1 s + \Gamma_0}{s^2 + 2\xi\omega_p s + \omega_p^2} \tag{7}$$

where ξ, ω_p, Γ_2, Γ_1, Γ_0 are the adjustable parameters of the controller. As a matter of fact, the term $C_{damp}{}^* y(t)$ can be regarded as the connection of the acceleration, velocity, and position signals $(\Gamma_2 s^2 + \Gamma_1 s + \Gamma_0) * y(t)$ and a low-pass filter $1/(s^2 + 2\xi\omega_p s + \omega_p^2)$, where Γ_2, Γ_1, and Γ_0 mean the weights of the feedback values of the acceleration, velocity, and position signals, respectively. As there only exists a position sensor in the system, the acceleration and velocity signals are derived by the first and second difference of the position signal, respectively. To avoid the amplification of the sensor noise in the difference process, the low-pass filter is thus employed. Therefore, the PAVPF controller is defined as the format of Eq. (7).

From Fig. 6, the transfer function of the damped system with PAVPF controller has the expression of

$$P_{damp}(s) = \frac{\hat{G}(s)}{1 - \hat{G}(s) C_{damp}(s)} = \frac{N(s)}{M(s)} \tag{8}$$

where $N(s)$ and $M(s)$ have the expressions

$$N(s) = (a_3 s^3 + a_2 s^2 + a_1 s + a_0)(s^2 + 2\xi\omega_p s + \omega_p{}^2) \tag{9}$$

$$\begin{aligned} M(s) &= (s^3 + b_2 s^2 + b_1 s + b_0)(s^2 + 2\xi\omega_p s + \omega_p^2) \\ &\quad -(a_3 s^3 + a_2 s^2 + a_1 s + a_0)(\Gamma_2 s^2 + \Gamma_1 s + \Gamma_0) \\ &= (1 - \Gamma_2 a_3) s^5 + (b_2 + 2\xi\omega_p - \Gamma_1 a_3 - \Gamma_2 a_2) s^4 \\ &\quad +(b_1 + \omega_p{}^2 - \Gamma_0 a_3 - \Gamma_1 a_2 - \Gamma_2 a_1 + 2\xi\omega_p b_2) s^3 \end{aligned}$$

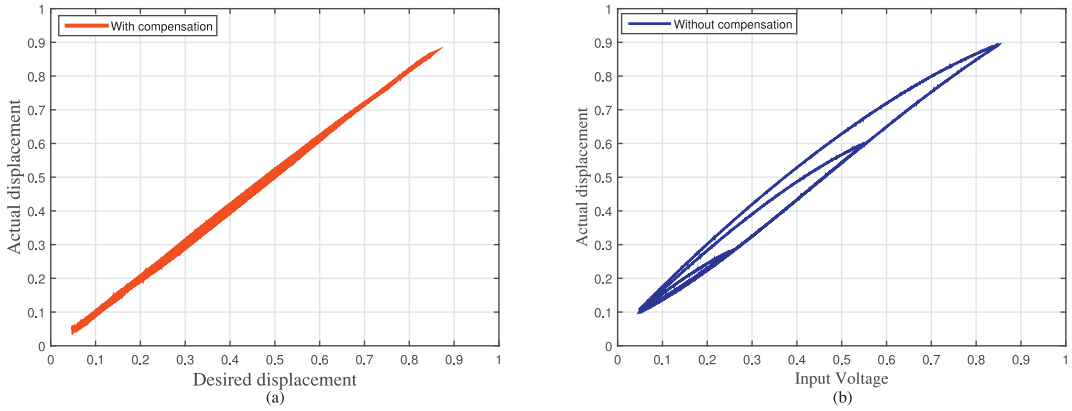

Fig. 4. Experimental results of the hysteresis curves for the system with and without the feedforward compensator: (a) with compensator; (b) without compensator.

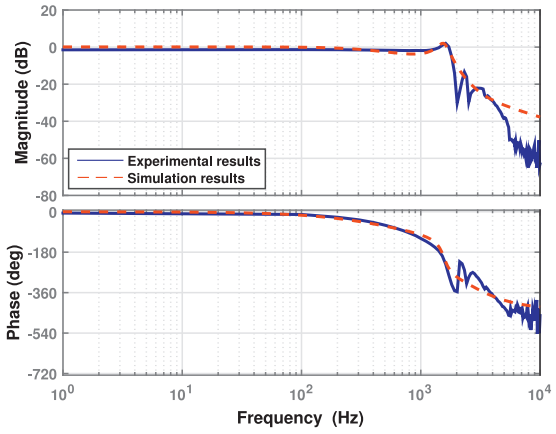

Fig. 5. The experimental frequency response and the frequency response of the identified simulation model.

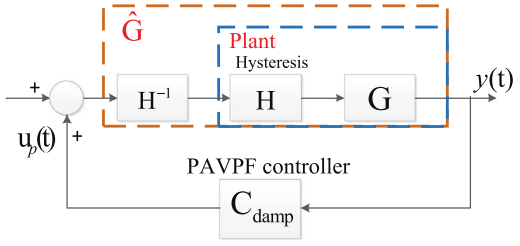

Fig. 6. The block diagram of the system with PAVPF control.

$$+(b_0-\Gamma_0a_2-\Gamma_1a_1-\Gamma_2a_0+2\xi\omega_{\mathrm{p}}b_1+b_2{\omega_{\mathrm{p}}}^2)s^2$$
$$+(2\xi\omega_{\mathrm{p}}b_0-\Gamma_1a_0-\Gamma_0a_1+b_1{\omega_{\mathrm{p}}}^2)s+b_0{\omega_{\mathrm{p}}}^2-\Gamma_0a_0 \quad (10)$$

It can be observed that Eq. (10) can be treated as a characteristic polynomial with five parameters $(\xi\omega_p, \omega_p^2, \Gamma_2, \Gamma_1, \Gamma_0)$. Meanwhile, there are five zeroes of the equation $M(s)=0$, which corresponds to the five poles of the damped system with PAVPF controller. Hence, from the view of mathematical principles, it is possible to allocate each pole of the damped system to a desired location arbitrarily. Provided that the desired locations of the poles are set as $P_i(i=1,2,3,4,5)$, the characteristic equation can be expressed as

$$\begin{aligned} Q(s) &= (s-P_1)(s-P_2)(s-P_3)(s-P_4)(s-P_5) \\ &= s^5+K_4s^4+K_3s^3+K_2s^2+K_1s+K_0 \end{aligned} \quad (11)$$

where

$$K_4 = -P_1-P_2-P_3-P_4-P_5$$
$$K_3 = P_3(P_2+P_1)+P_1P_2+P_4(P_3+P_2+P_1)$$
$$+P_5(P_4+P_3+P_2+P_1)$$
$$K_2 = -P_4(P_3P_1+P_3P_2+P_1P_2)-P_5[P_3P_1+P_3P_2+P_1P_2$$
$$+P_4(P_1+P_2+P_3)]-P_1P_2P_3$$
$$K_1 = P_5(P_4P_3P_1+P_4P_3P_2+P_4P_1P_2+P_1P_2P_3)+P_1P_2P_3P_4$$
$$K_0 = -P_1P_2P_3P_4P_5 \quad (12)$$

To assign the poles of the damped system to the desired locations $P_i(i=1,2,3,4,5)$, the coefficients of the characteristic polynomial $M(s)$ and the coefficients of $Q(s)$ should satisfy the following conditions:

$$K_4(1-\Gamma_2a_3) = b_2+2\xi\omega_{\mathrm{p}}-\Gamma_1a_3-\Gamma_2a_2$$
$$K_3(1-\Gamma_2a_3) = b_1+{\omega_{\mathrm{p}}}^2-\Gamma_0a_3-\Gamma_1a_2-\Gamma_2a_1+2\xi\omega_{\mathrm{p}}b_2$$
$$K_2(1-\Gamma_2a_3) = b_0-\Gamma_0a_2-\Gamma_1a_1-\Gamma_2a_0+2\xi\omega_{\mathrm{p}}b_1+b_2\omega_p^2$$
$$K_1(1-\Gamma_2a_3) = 2\xi\omega_pb_0-\Gamma_1a_0-\Gamma_0a_1+b_1\omega_p^2$$
$$K_0(1-\Gamma_2a_3) = b_0\omega_p^2-\Gamma_0a_0 \quad (13)$$

Eq. (13) can be expressed in the matrix form

$$\mathrm{A}\bullet X = B \quad (14)$$

where

$$X = (\xi\omega_{\mathrm{p}} \quad {\omega_{\mathrm{p}}}^2 \quad \Gamma_2 \quad \Gamma_1 \quad \Gamma_0)^T \quad (15)$$

$$A = \begin{pmatrix} 2 & 0 & -a_2+K_4a_3 & -a_3 & 0 \\ 2b_2 & 1 & -a_1+K_3a_3 & -a_2 & -a_3 \\ 2b_1 & b_2 & -a_0+K_2a_3 & -a_1 & -a_2 \\ 2b_0 & b_1 & K_1a_3 & -a_0 & -a_1 \\ 0 & b_0 & K_0a_3 & 0 & -a_0 \end{pmatrix} \quad (16)$$

$$\mathrm{B} = \begin{pmatrix} K_4-b_2 \\ K_3-b_1 \\ K_2-b_0 \\ K_1 \\ K_0 \end{pmatrix} \quad (17)$$

By solving the linear equation (14), the PAVPF controller can be obtained.

Based on the above principle, the PAVPF controller is designed for the system $\hat{G}$. The damping control objective is that the dominant poles have desired damping ratio. In this sense, the desired locations of the poles should be placed far to the left half plane. In this work, the desired poles are chosen as

$$\mathrm{p'}_{1,2,3,4} = -3000\pm 9806i \quad (18)$$

$$p'_5 = -2840 \quad (19)$$

which means that the desired damping ratio of the dominant pole is 0.297. Then, substituting Eqs. (18) and (19) into Eqs. (12) and (13), the solution of Eq. (14) can be obtained, which determines the adjustable parameters in Eq. (7). The obtained PAVPF damping controller can be expressed as:

$$C_{damp}(s) = \frac{0.2536s^2 + 5.360e3s + 1.318e7}{s^2 + 1.010e4s + 1.270e8} \tag{20}$$

3.3. PVPF damping controller

For a comparative study, the PVPF controller is designed with the same control objective to verify the damping performance of the PAVPF controller. For more details about the PVPF control and the design of the PVPF controller, readers may refer to [21,26]. The transfer function of the PVPF controller can be written as:

$$C_{PVPF}(s) = \frac{F_1 s + F_0}{s^2 + 2\xi_v \omega_v s + \omega_v{}^2} \tag{21}$$

Then, the characteristic equation of the damped system with PVPF control is

$$|1 - \hat{G}(s) C_{PVPF}(s)| = 0 \tag{22}$$

As discussed in [21,26], the PVPF control approach can place the poles of the damped system arbitrarily with an analytical method, when the model of the target system is second order. With the third model expressed in Eq. (4), the PVPF controller could not be designed directly to suppress the resonant vibration of the system using an analytical method. Therefore, a numerical method is chosen to optimize the control parameters of the PVPF controller.

For a fair comparison, the set point in this PVPF controller is the same with the one of the PAVPF controller in Eqs. (18) and (19). Since the real pole of the system does not influence the damping performance of the system, the objective function for the optimization method is expressed as

$$\min \ Fun = |Re(p''_{1234}) - Re(p'_{1234})| \tag{23}$$

where $Re(p''_{1234})$ is the real part of the objective complex poles. The Matlab optimization function 'lsqnonlin' is adopted to optimize the controller parameters. The determined transfer function is

$$C_{PVPF}(s) = \frac{5560s + 1.353e7}{s^2 + 9915s + 1.517e8} \tag{24}$$

With the simulation results, it can be obtained that the poles of the damped system with PVPF control are not exactly equal to the set point. However, with the PAVPF controller, the poles of the damped system can be assigned in an arbitrary manner accurately. For validating the effectiveness of the PAVPF controller, comparative experiments are performed as well. The frequency responses of experimental results of the system in open-loop, with PVPF controller and with PAVPF controller are compared in Fig. 7. It can be observed that the lightly damped resonant peak is well suppressed by both the PVPF controller and the PAVPF controller. The PAVPF controller has a more significant vibration suppression effect. Fig. 8 plots the step responses of the system in open-loop, with PVPF controller and with PAVPF controller, respectively. Based on the experimental results, the overshoot of the system with the PAVPF controller is smaller than that of the system without it. Meanwhile, the damping performance of the PAVPF controller is slightly better, compared with the PVPF controller. Therefore, the effectiveness of the PAVPF controller on damping control is demonstrated.

3.4. High-gain feedback controller

In this control approach, a feedback tracking controller is required to deal with the tracking errors. Therefore, a proportional-integral (PI) controller is used as the tracking controller in the outer feedback loop. The PI controller has the transfer function of $C_{track}(s) = k_p + k_i/s$, in which k_p and k_i are the proportional and integral gains, respectively. The block diagram of the system with PAVPF-based control approach is shown in Fig. 9. To determine the exact values of the gains k_p and k_i, the stability analysis of the system with PI+PAVPF is provided using a graphical method. For the detail algorithms of the graphical method, readers can refer to [27,35]. The stability region with the magnitude margin A of 9.5 dB and phase margin ϕ of 60° is shown in the intersection area of these two stability boundaries in Fig. 10. To optimize the control gains of the PI controller, the control bandwidth of the system with PI+PAVPF controller are analyzed. With every pair of k_p and k_i uniform distribution in the stability region, the control bandwidth of the system with different control gains is tested individually, based on the simulation results. The grey-scale map, as shown in Fig. 10, shows the simulation results of the control bandwidth in normalized case to illustrate the variation rule of the control bandwidth. It can be seen that the higher bandwidth exists in the region with the higher integral gain k_i. The control gains k_p and k_i will be determined in the stability region with a higher control bandwidth, by trial and error method in the experiment.

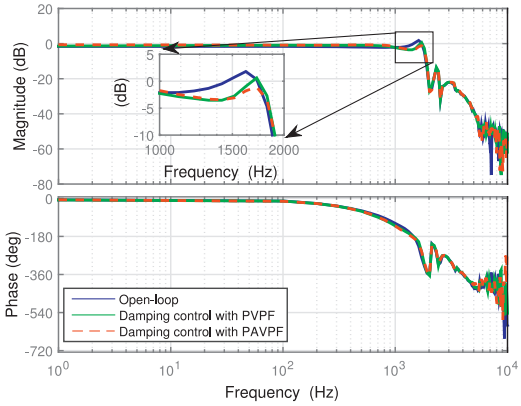

Fig. 7. The frequency responses of the system in open-loop, with PVPF, with PAVPF.

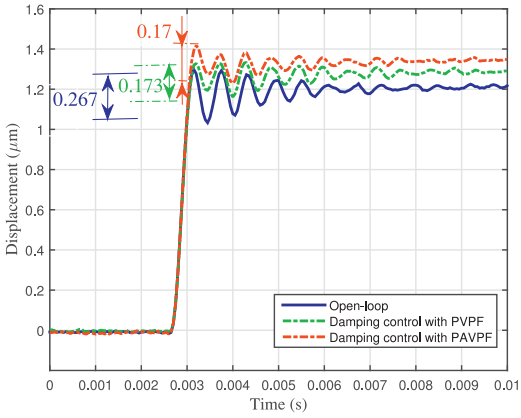

Fig. 8. The step responses of the system in open-loop, with PVPF, with PAVPF.

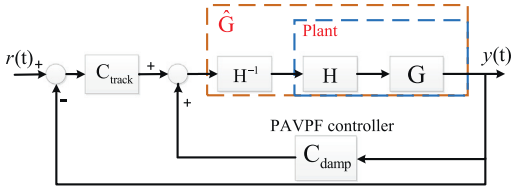

Fig. 9. The block diagram of overall control scheme of the system with PI + PAVPF.

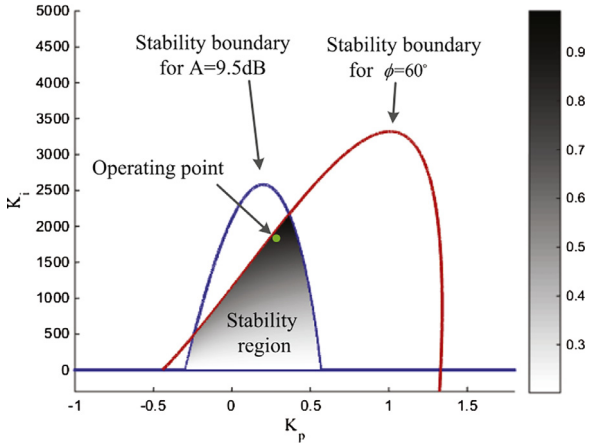

Fig. 10. The stability region of the system with PI+PAVPF for magnitude margin 9.5 dB and phase margin 60°. The grey-scale map in the figure is the control bandwidth in normalized case.

4. Experimental results

In this section, real-time experiments are performed on the experimental platform, as shown in Fig. 1, to verify the advantages of the proposed control approach.

Remark: With the similar damping performance of the PAVPF controller and the PVPF controller, the following bandwidth test results and the tracking performance of the system with PI+PVPF controller are close to the results of the system with PI+PAVPF controller, which is also verified by the real-time experiments. Therefore, the comparative experimental results of the system with PI+PVPF controller are not presented in this paper.

4.1. Bandwidth test

Firstly, experiments are performed to determine the control gains of the PI controller of the system with PI+PAVPF control. The control gains k_p and k_i are determined as 0.3 and 1900, respectively. The determined operating point can be found in Fig. 10, with the magnitude margin more than 9.5 dB and phase margin more than 60°. For comparison, experiments are performed with the traditional PI controller for the hysteresis compensated system. The hysteresis compensator of the system with PI control is the same with that of the system with PI+PAVPF control. The proportional and integral gains of the traditional PI controller are determined as $K_p = 0.3$ and $K_i = 800$, with trial and error method. The step responses of the system with PI+PAVPF controller and the system with PI controller are shown in Fig. 11. The output of the system with PI control exhibits obvious oscillations, and converges slowly with rising time of about 2.8 ms and settling time of about 5 ms. In contrast, the rising time and settling time of the PI+PAVPF control are about 0.45 ms and 2 ms, respectively. These characteristics show great superiorities of the PI+PAVPF controller on the transient response.

Furthermore, experiments are performed to test the control bandwidth of the system with these two control approaches. With this objective, the band-limited white noise signal is also selected to stimulate the system with PI controller and with PI+PAVPF controller, respectively. The crossover frequency at -3 dB, which is generally chosen as a measurement of the system bandwidth [36], is selected as the index of control bandwidth. The frequency responses of these two closed-loop systems (with PI controller and with PI+PAVPF controller) are shown in Fig. 12. The bandwidths of the system with PI controller and with PI+PAVPF controller are 111 Hz and 766 Hz, respectively. It can be obtained that the control bandwidth of system with PI +PAVPF controller improves about 6 times, which validates the advantages of the proposed PAVPF controller.

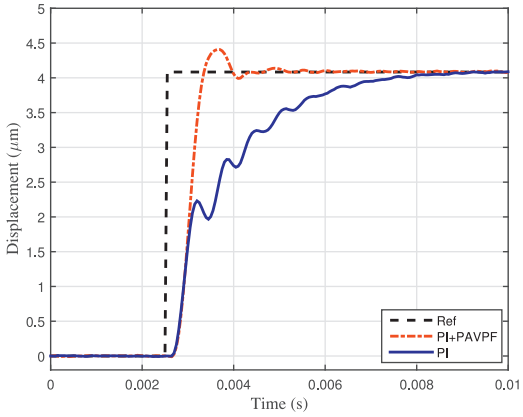

Fig. 11. Step responses of system with PI and PI+PAVPF controller.

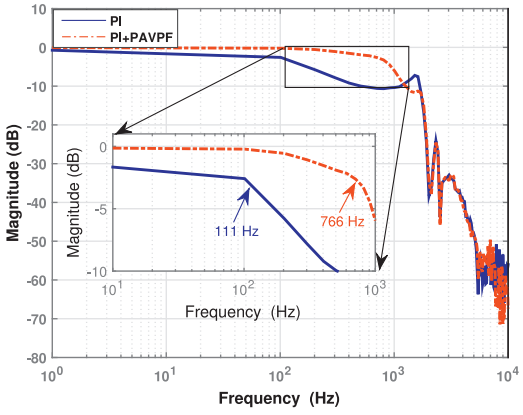

Fig. 12. Frequency responses of the system with PI and with PI+PAVPF control.

4.2. Tracking performance

The control objective of a nanopositioning stage is to accurately track a predefined trajectory. In most practical applications, most of the tasks for the stage are to track a periodic triangular trajectory [2,7,37–39]. Hence, real-time triangular trajectories tracking experiments are conducted with typical fundamental frequencies of 1, 10, 50 and 100 Hz, respectively. Fig. 13(a) and (b) illustrate the comparison of the tracking performance of the system with PI controller and with PI+PAVPF controller, under 50 Hz and 100 Hz triangular trajectories, respectively. As shown in Fig. 13, the tracking performance of the system with the PI+PAVPF controller is improved significantly, by comparing to the tracking results of the system with PI controller. Besides, as described in Fig. 13, tracking performances of both the PI controller and the PI+PAVPF controller degrade, as the increase of the input signal frequency, which is influenced by the limited bandwidth of the controlled system.

With the objective of quantifying the tracking results of the PAVPF-based control approach, two indexes are chosen as follows:

$$e_m = \frac{\max\limits_{t\in[0,2T)} |y(t) - r(t)|}{\max(r(t)) - \min(r(t))} \times 100\% \tag{25}$$

$$e_{rms} = \frac{\sqrt{\frac{1}{2T}\int_0^{2T} [y(t) - r(t)]^2 dt}}{\max(r(t)) - \min(r(t))} \times 100\% \tag{26}$$

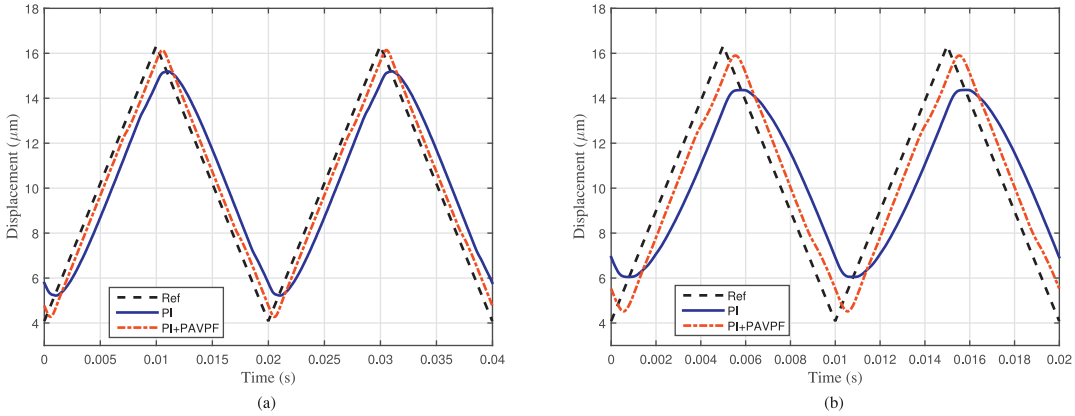

Fig. 13. Comparisons of the triangular trajectory tracking results of the stage with different control method with different fundamental frequencies: (a) 50 Hz; (b) 100 Hz.

Table 2
Obtained tracking errors of the tracking experiments with different fundamental frequencies for different control approaches.

Frequency (Hz)	PI		PI+PAVPF	
	$e_m(\%)$	$e_{rms}(\%)$	$e_m(\%)$	$e_{rms}(\%)$
1	0.39	0.25	0.21	0.09
10	2.53	3.07	1.23	0.96
50	13.93	10.91	5.95	4.84
100	23.35	18.12	11.80	9.37

where $r(t)$ represents the input signal as reference signal, $y(t)$ represents the actual output position signal, and T denotes the cycle of the input signal. e_m and e_{rms} indicate the maximum tracking error and the root mean square tracking error of the stage, respectively. For comparison, e_m and e_{rms} of the system with different control approaches in the tracking experiments are summarized in Table 2. It is clearly seen that the tracking errors of the system with PI+PAVPF controller are reduced significantly, when comparing to the system with PI controller. In this sense, the advantage of the PAVPF-based control approach is demonstrated on high-bandwidth tracking control.

5. Conclusion

In this work, a PAVPF control approach is presented to suppress the vibration of the resonant mode of piezo-actuated nanopositioning stage to achieve high-bandwidth control. The PAVPF-based control approach is composed of the hysteresis compensator, the PAVPF controller, and the tracking controller. The hysteresis compensator with a MPI model is introduced for dealing with the nonlinearity of the PEA, which leads to an approximately linear system. The pole-placement method is utilized to design the PAVPF controller, which adds sufficient damp to the lightly damped system. Then, a PI controller is designed to enhance the tracking performance of the nanopositioning stage. Finally, to evaluate the advantages of the PAVPF-based control approach, comparative experiments with PVPF controller and with conventional PI controller are performed. Experimental results demonstrate that the performance with the PI+PAVPF controller is improved significantly.

Acknowledgments

This work was partially supported by the National Natural Science Foundation of China under Grant Nos. 51405293 and 91648202, and the Specialized Research Fund for the Doctoral Programme of Higher Education under Grant No. 20130073110037.

References

[1] Devasia S, Eleftheriou E, Moheimani SOR. A survey of control issues in nanopositioning. IEEE Trans Control Syst Technol 2007;15(5):802–23.
[2] Salapaka SM, Salapaka MV. Scanning probe microscopy. IEEE Control Syst Maganize 2008;28(2):65–83.
[3] Ando T, Uchihashi T, Fukuma T. High-speed atomic force microscopy for nano-visualization of dynamic biomolecular processes. Prog Surf Sci 2008;83(7–9):337–437.
[4] Yang YL, DWei Y, Lou JQ, Tian G, Zhao XW, Fu L. A new piezo-driven microgripper based on the double-rocker mechanism. Smart Mater Struct 2015;24(7):075031.
[5] Wang FJ, Liang CM, Tian YL, Zhao XY, Zhang DW. Design of a piezoelectric-actuated microgripper with a three-stage flexure-based amplification. IEEE/ASME Trans Mechatron 2015;20(5):2205–13.
[6] Croft D, Shed S, Devasia S. Creep, hysteresis, and vibration compensation for piezoactuators: atomic force microscopy application. J Dyn Syst Meas Control 2001;123(1):35–43.
[7] Eielsen AA, Vagia M, Gravdahl JT, Pettersen KY. Damping and tracking control schemes for nanopositioning. IEEE Trans Mechatron 2014;19(2):432–44.
[8] Gu GY, Zhu LM, Su CY, Ding H, Fatikow S. Modeling and control of piezo-actuated nanopositioning stages: a survey. IEEE Trans Autom Sci Eng 2016;13(1):313–32.
[9] Hassani V, Tjahjowidodo T, Do TN. A survey on hysteresis modeling, identification and control. Mech Syst Signal Process 2014;49(1–2):209–33.
[10] Clayton GM, Tien S, Leang KK, Zou QZ, Devasia S. A review of feedforward control approaches in nanopositioning for high-speed SPM. J Dyn Syst Meas Control 2009;131(6):061101.
[11] Gu GY, Zhu LM, Su CY, Ding H. Motion control of piezoelectric positioning stages: modeling, controller design, and experimental evaluation. IEEE Trans Mechatron 2013;18(5):1459–71.
[12] Fleming AJ, Leang KK. Charge drives for scanning probe microscope positioning stages. Ultramicroscopy 2008;108(12):1551–7.
[13] Qin YD, Tian YL, Zhang DW, Shirinzadeh B, Fatikow S. A novel direct inverse modeling approach for hysteresis compensation of piezoelectric actuator in feedforward applications. IEEE/ASME Trans Mechatron 2013;18(3):981–9.
[14] Xu QS, Wong PK. Hysteresis modeling and compensation of a piezostage using least squares support vector machines. Mechatronics 2011;21(7):1239–51.
[15] Krejci P, Kuhnen K. Inverse control of systems with hysteresis and creep. IEE Proc - Control Theory Appl 2001;148(3):185–92.
[16] Guo ZY, Tian YL, Liu XP, Shirinzadeh B, Wang FJ, Zhang DW. An inverse Prandtl-Ishlinskii model based decoupling control methodology for a 3-DOF flexure-based mechanism. Sens Actuators A 2015;230:52–62.
[17] Shan JJ, Liu YF, Gabbert U, Cui NG. Control system design for nano-positioning using piezoelectric actuators. Smart Mater Struct 2016;25(2):025024.
[18] Fanson JL, Caughey TK. Positive position feedback control for large space structures. AIAA J 1990;28(4):717–24.
[19] San-Millan A, Russell D, Feliu V, Aphale SS. A modified positive velocity and position feedback scheme with delay compensation for improved nanopositioning performance. Smart Mater Struct 2015;24(7):075021.
[20] Omidi E, Mahmoodi N. Hybrid positive feedback control for active vibration attenuation of flexible structures. IEEE Trans Mechatron 2015;20(4):1790–7.
[21] Bhikkaji B, Ratnam M, Moheimani SOR. PVPF control of piezoelectric tube scanners. Sens Actuators A 2007;135(2):700–12.
[22] Mahmoodi SN, Ahmadian M. Active vibration control with modified positive position feedback. J Dyn Syst Meas Control 2009;131(4):041002.
[23] Fleming AJ. Nanopositioning system with force feedback for high-performance tracking and vibration control. IEEE Trans Mechatron 2010;15(3):433–47.
[24] Al-Mamun A, Keikha E, Bhatia CS, Lee TH. Integral resonant control for suppression of resonance in piezoelectric micro-actuator used in precision servomechanism. Mechatronics 2013;23(1):1–9.

[25] Aphale SS, Fleming AJ, Moheimani SOR. Integral resonant control of collocated smart structures. Smart Mater Struct 2007;16(2):439.
[26] Bhikkaji B, Ratnam M, Fleming AJ, Moheimani SOR. High-performance control of piezoelectric tube scanners. IEEE Trans Control Syst Technol 2007;15(5):853–66.
[27] Yang MJ, Niu JB, Li CX, Gu GY, Zhu LM. High-bandwidth control of nanopositioning stages via an inner-loop delayed position feedback. IEEE Trans Autom Sci Eng 2015;12(4):1357–68.
[28] Ratnam M, Bhikkaji B, Fleming AJ, Moheimani SOR. PPF control of a piezoelectric tube scanner. In: Proceedings of the 44th IEEE conference on decision and control; 2005. p. 1168–73.
[29] Song GB, Agrawal BN. Vibration suppression of flexible spacecraft during attitude control. Acta Astronaut 2001;49(2):73–83.
[30] Das SK, Pota HR, Petersen IR. Damping controller design for nanopositioners: a mixed passivity, negative-imaginary, and small-gain approach. IEEE Trans Mechatron 2015;20(1):416–26.
[31] Boukari AF, Carmona JC, Moraru G, Malburet F, Chaaba A, Douimi M. Piezo-actuators modeling for smart applications. Mechatronics 2011;21(1):339–49.
[32] Leang KK, Fleming AJ. Tracking control for nanopositioning systems. In: Nanopositioning technologies: fundamentals and applications. Springer International Publishing; 2016. p. 213–44.
[33] Gu GY, Yang MJ, Zhu LM. Real-time inverse hysteresis compensation of piezoelectric actuators with a modified Prandtl-Ishlinskii model. Rev Sci Instrum 2012;83(6):065106.
[34] Yang MJ, Gu GY, Zhu LM. Parameter identification of the generalized Prandtl-Ishlinskii model for piezoelectric actuators using modified particle swarm optimization. Sens Actuators A 2013;189:254–65.
[35] Tan N, Kaya I, Atherton DP. A graphical method for computation of all stabilizing pi controllers. IFAC Proc Vol 2005;38(1):349–54.
[36] Kenton BJ, Leang KK. Design and control of a three-axis serial-kinematic high-bandwidth nanopositioner. IEEE Trans Mechatron 2012;17(2):356–69.
[37] Gu GY, Zhu LM, Su CY, Ding H, Fatikow S. Proxy-based sliding-mode tracking control of piezoelectric-actuated nanopositioning stages. IEEE/ASME Trans Mechatron 2015;20(4):1956–65.
[38] Bazaei A, Chen Z, Yong YK, Moheimani SOR. A novel state transformation approach to tracking of piecewise linear trajectories. IEEE Trans Control Syst Technol 2017;PP(99):1–11.
[39] Maroufi M, Bazaei A, Moheimani SOR. A High-Bandwidth MEMS Nanopositioner for On-Chip AFM: Design, Characterization, and Control. IEEE Trans Control Syst Technol 2015;23(2):504–12.

Linlin Li received the B.E. degree (with honors) in Mechanical design, manufacturing and automation from Shandong University, Jinan, China, in 2014. She is currently working toward the Ph.D. degree in mechanical engineering at Shanghai Jiao Tong University, Shanghai, China.

Her research interests include mechatronics, modeling and control of high-bandwidth nanopositioning stages.

Chun-Xia Li received the B.E. degree (with honors) in mechanical engineering from Shanghai Jiao Tong University, Shanghai, China, in 2011, where she is currently working toward the Ph.D. degree in mechanical engineering. Her research interests include compliant mechanisms, design and control of high-bandwidth nanopositioning stages.

Miss Li was a recipient of the National Scholarship for Excellent Master Student granted by Ministry of Education of China in 2012.

Guoying Gu received the B.E. degree (with honors) in electronic science and technology, and the Ph.D. degree (with honors) in mechatronic engineering from Shanghai Jiao Tong University, Shanghai, China, in 2006 and 2012, respectively. Dr. Gu was a Visiting Scholar at Concordia University, Montreal, QC, Canada, and National University of Singapore, Singapore. Supported by the Alexander von Humboldt Foundation, he was as a Humboldt Fellow at University of Oldenburg, Oldenburg, Germany. Since October 2012, he has worked at Shanghai Jiao Tong University, where he is currently appointed as an Associate Professor with School of Mechanical Engineering. His research interests include soft robots and high precision motion control. He is the author or co-author of over 40 publications, which have appeared in journals, as book chapters and in conference proceedings.

Dr. Gu is a member of the American Society of Mechanical Engineers. Now Dr. Gu serves as Associate Editor of International Journal of Advanced Robotic Systems. He has also served for several international conferences as Associate Editor or an program committee member.

Li-Min Zhu received the B.E. degree (with honors) and the Ph.D. degree in mechanical engineering from Southeast University in 1994 and 1999, respectively. From Nov. 1999 to Jan. 2002, he worked as a postdoctoral fellow in Huazhong University of Science and Technology. Since March 2002, he has been with Shanghai Jiao Tong University. He is currently the Cheung Kong Chair Professor, Head of the Department of Mechanical engineering and Automation, and Vice Director of the State Key Laboratory of Mechanical System and Vibration. His research interests include: (1) Modeling and control of smart materials-based actuators, (2) Control, sensing and instrumentation for micro/nano manufacturing, (3) Motion control and trajectory generation for CNC machine tools, (4) Mechanics and dynamics of machining operation for process optimization, monitoring and control, and (5) Coordinate measurement and computational metrology.

Prof. Zhu was the recipient of the National Science Fund for Distinguished Young Scholars in 2013 and selected into the National High-level Personnel of Special Support Program in 2016. He has published one monograph and more than 200 peer reviewed papers, including 122 on international journals. He is now an Associate Editor for the IEEE Transactions on Automation Science and Engineering, a Technical Editor for the IEEE/ASME Transactions on Mechatronics, and Editorial Board Members of the Proceedings of the Institution of Mechanical Engineer (IMechE), Part B: Journal of Engineering Manufacture and the International Journal of Intelligent Robotics and Applications.